Identification methodology of a rate-sensitive constitutive law with mean field and full field modeling approaches for polycrystalline materials

Yann Charles, Chunping Zhang, Monique Gaspérini, Brigitte Bacroix

Identification methodology of a rate sensitive constitutive law with mean field and full field modelling approaches for polycrystalline materials.

Yann Charles[1], Chunping Zhang[2], Monique Gaspérini[1], Brigitte Bacroix[3,*]

[1] Université Sorbonne Paris Nord, Laboratoire des Sciences des Procédés et des Matériaux, LSPM, CNRS, UPR 3407, F-93430, Villetaneuse, France,

[2] Now at Département de Génie Mécanique, École de Technologie Supérieure, 1100 Rue Notre-Dame Ouest, Montréal, QC H3C 1K3, Canada

[3] CNRS, UPR3407, Laboratoire des Sciences des Procédés et des Matériaux, LSPM, Université Sorbonne Paris Nord, F-93430, Villetaneuse, France,

[*] Corresponding author

Emails: yann.charles@univ-paris13.fr, chunping.zhang.1@gmail.com, gasperini@univ-paris13.fr, brigitte.bacroix@lspm.cnrs.fr

Abstract: the present paper deals with the consideration of the rate sensitivity mechanical behavior of metallic materials, in the framework of mean field and full field homogenization approaches. We re-examine the possibility of describing properly this rate sensitivity with a simple and widely used power law expressed at the level of the slip system, and we propose a methodology to accelerate the identification of the global material constitutive law for Finite Element (FE) simulations. For such an aim, simulations of a tensile test are conducted, using a simple homogenization model (the Taylor one, used in a relaxed constraint form) and a FE code (Abaqus), both using the same single-crystal rate-dependent constitutive law. It is shown that, provided that the identification of this law is performed with care and well adapted to the examined case (rate sensitive or insensitive materials, static and/or dynamic ranges), the simple power law can be used to simulate the macroscopic behavior of polycrystalline aggregates in a wide range of strain rate (including both static and dynamic regimes) and strain rate sensitivity (up the rate-insensitive limit).

Keywords: viscoplasticity, polycrystalline materials, strain-rate sensitivity, Finite Element.

1. Introduction

For the modelling of the global and local mechanical behaviors of polycrystalline metals in a wide range of temperature or strain rate – with polycrystalline models, such as Taylor [1-3] or Self Consistent models [4-6], with finite element (FE) codes [7-10], or with multiscale approaches coupling DDD (Discrete Dynamic Dislocations) approaches with FE codes [11, 12] – it is quite usual to use a rate-dependent crystalline constitutive law, which generally takes the form of the following power law expressed on the slip system s [1][a]

$$\dot{\gamma}^s = \dot{\gamma}_0^s \left(\frac{\tau^s}{\tau_0^s} \right)^n \tag{1}$$

In this expression, n (or more often $1/n = m$) characterizes the material rate sensitivity, $\dot{\gamma}^s$ is the slip rate, and τ^s the resolved shear stress. The term τ_0^s is the so-called critical (or reference) resolved shear stress (which evolves with strain when hardening is considered), while the parameter $\dot{\gamma}_0^s$ is usually called a reference shear rate [7, 8, 12]. If the exponent n is the same for all systems and for all grains of a polycrystal, it is easy to show that this exponent is also the macroscopic rate sensitivity of the polycrystal as a whole [2]. By assuming the rate dependence at the slip system level, this widely accepted phenomenological law presents the double advantage of (i) assuming that plastic strain occurs solely by crystallographic slip on well-defined slip systems, which is generally true for most metals at not too high temperatures and (ii) suppressing the long standing problem of non-uniqueness in the choice of active slip systems usually encountered in rate-independent crystalline plasticity [13-15].

Such a viscoplastic crystalline law has also been shown to be able to provide physically based large-strain rate-sensitive constitutive models, in order to interpret experiments on metals performed up to quite large strain-rates (up to 10^4 s^{-1}, see e.g. [10]), in which localization of plastic deformation is observed. Indeed, although rate sensitivity may be neglected on purpose for many metallic alloys cold-deformed at low strain rates and strains, this may no longer be valid when moderate or high strain rates are applied, or when high temperature data are considered. It is now well-known that, in such a case, the resulting

[a] By using only odd values of the exponent n, we avoid in the formulation the use of absolute values. Thus, the more classically chosen value of 20 will be replaced here by 21, since the resulting difference in the macroscopic behaviour is hardly detectable.

localization of plastic flow is indeed strongly influenced by the strain-rate sensitivity of the material [16-18], and to a lesser extent by the deformation induced anisotropy [19]. Actually, many authors have observed an increased rate sensitivity at large applied strain rates, and have postulated that this rate sensitivity increase is a characteristic of the material [1, 10, 20, 21]. How large the strain rate must be to observe this increased rate sensitivity is still not clear, however. Indeed, the strain rate sensitivity depends in quite a complex way on strain rate, but also on strain, temperature, as well as on the underlying microstructure and possible deformation mechanisms of the tested materials [6, 22-24]. Thus, a lot of successful modelling efforts, some of them based on the very same power law as the one defined in Eq. 1, have been made to be able to simulate different strain rate regimes, either controlled by the thermally activated interactions between dislocations at rather low strain rates or by dislocation drag at high strain rates (see, e.g. [25-28]). Conversely, some other authors claim that accounting for rate sensitivity solely by a single relationship between shear rate and shear stress is a too simplified approach even for low strain rates, and that this approach should be replaced or completed by a rate-sensitive hardening law, describing the evolution of τ_0^s with strain and strain-rate (e.g. [9, 29, 30]), to account for the right influence of strain-rate sensitivity on the behavior of polycrystalline materials. Additionally, since this classical power law is still mostly used with the aim of simplifying the numerical procedures by providing a regularized form (with a unique solution on a given slip system) of the slip criterion, the exponent n is usually not correctly set up (see below), resulting in an inaccurate coupling between the macroscopic rate sensitive response and the rate sensitive evolutions of critical resolved shear stresses of slip systems. In order to solve this problem for rate-sensitive or rate-insensitive materials, some much more numerically efficient methods have been recently proposed [29, 31]. The first one [29] aims at describing properly the behavior of materials in a wide range of rate-sensitivity and strain-rate, whereas the second one [31] aims at being able to treat efficiently the case of rate–insensitive materials. However, according to the authors themselves, these efficient methods are not adapted either to the treatment of rate-sensitive materials [31] or to their combined used with FE codes [32].

Thus, and especially in the framework of FE simulations, a lot of works are still based on the use of the classical viscoplastic crystalline power law (Eq. 1), partly also rendered popular by the UMAT (User Material) subroutine developed by Huang for the commercial software Abaqus [33]. However, even in some very recent papers, the exponent of rate sensitivity is set without any justification (e.g. [12]) or is *assumed* to be "adequately chosen to neglect the rate-

sensitivity" (e.g. [8, 16, 34]) at the polycrystal scale. In fact, it is easy to show that it is not the case for many of the reported simulations, and that the choice made leads precisely to unexpected high strain-rate sensitivity, as soon as the strain rate varies.

The aim of the present paper is thus to re-address the question, and the use, of the applied strain-rate sensitivity in computations using a power law based crystal plasticity model, for both rate-insensitive and rate-sensitive materials. We will first **recall the procedure to use adequately such a simple formulation for rate-insensitive materials**. With the addition of the phenomenological saturating hardening law used in [33], we will then **propose a methodology to accelerate the identification of the parameters describing the constitutive law of the material, with a FE code, for rate-sensitive materials at rather low strain rates (i.e. within the static regime). We will finally show that this identification can be extended to the case of high strain rates (dynamic regime), provided that the *n* value is identified differently in both regimes**. This will be illustrated by some simulations of a tensile test performed using two different modelling approaches, i.e, a simple homogenization model (the Taylor one, used in a relaxed constraint form) and a FE computation (using Abaqus software and dedicated User Subroutines [33]), both approaches using the very same single-crystal rate-dependent constitutive law and allowing strain rate fluctuations within the polycrystalline material.

The outline of the present paper is thus the following: the classical single crystal viscoplastic flow rule and associated hardening law are presented in **Section 2**, its implementation into the Taylor model and FE Abaqus code are briefly described in **Sections 3 and 4**, the results of the performed simulations are then analyzed in **Section 5** and some conclusions are drawn in **Section 6**.

2. The classical single crystal viscoplastic flow rule and associated hardening law

As already mentioned, when a grain *g* of a polycrystalline sample is subjected to a stress state $\boldsymbol{\sigma}$, plastic strain takes place by slip on several slip systems, each labeled by index *s*. At the level of the slip systems, the rate dependent slip criterion is given by Eq. 1. The resolved shear stress on system *s* is equal to $\tau^s = \sigma_{ij} R^s_{ij} = S_{ij} R^s_{ij}$, $\boldsymbol{S}$ being the (symmetrical) deviatoric

stress tensor and $\boldsymbol{R}^s$ the orientation tensor of system s[b]. The components of this last tensor read

$$R_{ij}^s = \frac{1}{2}(n_i^s b_i^s + b_i^s n_i^s) \tag{2}$$

with $\vec{n}_s$ and $\vec{b}_s$ characterizing respectively the slip plane normal and the slip direction for the system *s*. The strain rate tensor $\dot{\boldsymbol{\varepsilon}}$ in grain *g* is then defined as a summation of individual shear-rate components on all systems *s*:

$$\dot{\varepsilon}_{ij} = \sum_s \dot{\gamma_0^s} \left(\frac{\tau^s}{\tau_0^s}\right)^n R_{ij}^s = \sum_s \dot{\gamma_0^s} \left(\frac{S_{kl}R_{kl}^s}{\tau_0^s}\right)^n R_{ij}^s \tag{3}$$

As long as the parameters τ_0^s, $\dot{\gamma_0^s}$ and the exponent of rate sensitivity *n* are constant, this equation represents a unique relationship between strain rate and deviatoric stress tensors at the level of grain *g,* which allows to determine both tensors from the boundary conditions imposed to the considered grain (more precisely 5 independent components for each tensor). The existence of a unique solution has the direct consequence that the current stress state vary with strain rate and vice versa. This constitutive law is classically accompanied by a hardening law, which can be expressed – again at the level of the slip systems – as

$$\dot{\tau}_0^s = \sum_l H_{sl}\dot{\gamma}^l \tag{4}$$

with H_{sl} the components of the so-called hardening matrix. As in the UMAT subroutine developed for Abaqus, a saturating expression – which has proven its efficiency to reproduce experimental data concerning several metallic alloys [35, 36] – can be adopted which reads

$$\begin{cases} H_{ss} = h_0 \operatorname{sech}^2 \left|\dfrac{h_0\bar{\gamma}}{\tau_{sat} - \tau_{ini}}\right| \\ H_{sl,\ s\neq l} = q h_0 \operatorname{sech}^2 \left|\dfrac{h_0\bar{\gamma}}{\tau_{sat} - \tau_{ini}}\right| \end{cases} \tag{5}$$

where $\bar{\gamma}$ is the cumulated shear strain on system s so that

[b] In the following, tensors are written in bold, and the subscript 'M' denotes macroscopic values.

$$\bar{\gamma} = \int_0^t \sum_s |\dot{\gamma}^s| dt \tag{6}$$

In order to characterize completely these laws (Eqs. 5 and 3), 4 material parameters are thus needed, namely τ_{ini}, τ_{sat}, q and h_0, together with two other sets of material parameters, τ_{0ini}^s (initial values) and $\dot{\gamma}_0^S$ – which can be reduced to 2 parameters τ_{0ini} and $\dot{\gamma}_0$ if they are assumed equal for all systems in all grains – and finally the exponent of rate sensitivity n. If one single value τ_{0ini} is imposed for all systems, then it is trivial to set it equal to τ_{ini}. In that case, the τ_{ini} and τ_{sat} values are directed linked to the initial and final values of both microscopic (at the level of the grain) and macroscopic stress values (see Figure 1 below). As for the h_0 hardening coefficient, it affects the hardening rate all along the stress – strain curve before the saturation level is reached (see again Figure 1).

Now, in order to demonstrate the usefulness of the proposed crystalline law, we are going to use two different simulations approaches (i.e., mean and full field ones) to calculate the macroscopic response of a polycrystalline aggregate in uniaxial tension; for both approaches, by construction, the local strain rate is allowed to differ from one grain to another and thus may be quite different from the macroscopic imposed one.

3. Simulation framework

3.1 The Taylor model (with full or relaxed constraints)

In the framework of the Taylor model (FC – Full Constraint or RC – Relaxed Constraint), several options are possible to simulate a tensile test along, e.g., the axis 3 of the macroscopic reference system:

(i) the Taylor model in the FC mode, which implies that all components of the strain rate tensor within each grain are assumed to be the same than the imposed macroscopic ones, i.e. $\dot{\boldsymbol{\varepsilon}} = \dot{\boldsymbol{E}}_{\mathrm{M}}$. For a general anisotropic material, the combined boundary conditions in terms of stress and strain rate then read at the level of the grain

$$\dot{\boldsymbol{\varepsilon}} = \dot{E}_{33_{imp}} \begin{vmatrix} -\alpha & 0 & 0 \\ 0 & 1-\alpha & 0 \\ 0 & 0 & 1 \end{vmatrix} \quad \text{and} \quad \boldsymbol{\sigma} = \begin{vmatrix} 0 & ? & ? \\ ? & 0 & ? \\ ? & ? & ? \end{vmatrix} \tag{7}$$

in which $\dot{E}_{33_{imp}}$ is the imposed macroscopic strain rate along the tensile axis and α the so-called contraction ratio, which has to be calculated, for each calculation step, by

minimizing the macroscopic plastic work rate with respect to α [37]. If the material is isotropic, this factor is set to be equal to 0.5 and no extra minimization procedure is necessary in this case. This case is known to represent an upper bound for the macroscopic behavior of the material.

(ii) the Taylor model in its most relaxed version, often called the Sachs–Köchendorfer model [38, 39]. In this case, a uniaxial stress state is applied to each grain, and only the macroscopic strain rate along the tensile axis $\dot{E}_{33}$ is imposed in each grain. The boundary conditions are then

$$\dot{\boldsymbol{\varepsilon}} = \dot{E}_{33_{imp}} \begin{vmatrix} ? & ? & ? \\ ? & ? & ? \\ ? & ? & 1 \end{vmatrix} \quad \text{and} \quad \boldsymbol{\sigma} = \begin{vmatrix} 0 & 0 & 0 \\ 0 & 0 & 0 \\ 0 & 0 & ? \end{vmatrix} \tag{8}$$

This option is usually applied for small strains, but it is considered to be far from the reality for moderate or large ones. It is worth mentioning that, as one of the 5 independent components of the strain-rate tensor is still imposed to each grain, this model does not corresponds to the so-called static model which constitutes the lower bound for the macroscopic behavior and for which the total stress tensor is the same for all grains.

(iii) an "intermediate" approach (which will be called RC – Relaxed Constraints – Taylor model in the following), which is thought to be better for anisotropic materials although quite simplified, which consists in allowing the contraction ratio α to be different within each grain, which implies the following boundary conditions

$$\dot{\boldsymbol{\varepsilon}} = \dot{E}_{33_{imp}} \begin{vmatrix} ? & 0 & 0 \\ 0 & ? & 0 \\ 0 & 0 & 1 \end{vmatrix} \quad \text{and} \quad \boldsymbol{\sigma} = \begin{vmatrix} 0 & ? & 0 \\ ? & 0 & ? \\ ? & ? & ? \end{vmatrix} \tag{9}$$

It is easy to prove that, if the sample is isotropic, we will get $\dot{E}_{M22} = \dot{E}_{M11} = 0.5$ at the level of the polycrystal and the resulting macroscopic stress state will also be purely uniaxial (like in the FC mode). Apart from being simpler and more rapid that the FC one, this version is thought to be especially well adapted to the simulation of a tensile test applied on anisotropic materials (as well as in isotropic ones of course) [40], and is consequent used in the present work.

For all these cases, it is readily seen that, among the 10 independent components of $\dot{\boldsymbol{\varepsilon}}$ and $\boldsymbol{\sigma}$ which need to be determined, 5 are imposed and the 5 remaining are deduced from Eq. 3. The associated macroscopic quantities $\dot{\boldsymbol{E}}_{\mathrm{M}}$ and $\boldsymbol{\Sigma}_M$ are then obtained by averaging on all grains.

Once the boundary conditions have been selected, an iterative calculation can be

performed to simulate a tensile test, and, from the boundary conditions expressed by Eq. 9 and the resolution of Eq. 3, the tensile deviatoric stress S_{33} and strain rate $\dot{\varepsilon}_{33} = \dot{E}_{33_{imp}}$ can be extracted at each step of the calculation (characterized by a time increment Δt). Then, at a given time *t* of the simulation, the total tensile strain can be obtained:

$$\Delta E_{33} = \dot{E}_{33_{imp}} \Delta t \;\Rightarrow\; E_{33}(t + \Delta t) = E_{33}(t) + \dot{E}_{33_{imp}} \Delta t \tag{10}$$

At each step, the reference shear stress of each system, within each grain, is also updated

$$\tau_0^s(t + \Delta t) = \tau_0^s(t) + \sum_l H_{sl} \dot{\gamma}^l(t)\, \Delta t \tag{11}$$

noting that, at time t=0, $\tau_0^s = \tau_{ini}$ and $\sum_l H_{sl} \dot{\gamma}^l(t) = 0$.

In order to calculate the macroscopic tensile curve, the deviatoric stress is averaged on all grains at each step to get $\boldsymbol{S}_M$ and the macroscopic true tensile stress Σ_{M33}. As

$$S_{Mii} = \langle S_{ii} \rangle \quad and \quad \Sigma_{Mii} = S_{Mii} + \frac{P}{3} \tag{12}$$

where P is the hydrostatic pressure, and since the macroscopic boundary conditions also impose that

$$\Sigma_{M11} = \Sigma_{M22} = 0 \tag{13}$$

then, we simply get

$$\Sigma_{M33} = \frac{3}{2} S_{M33} \tag{14}$$

Eqs. (10) and (14) allow then to plot the macroscopic tensile stress – strain curve. Since $\dot{E}_{33_{imp}}$ is imposed and constant along the test, the final strain can be written as

$$E_{33final} = \dot{E}_{33_{imp}} N_{step} \Delta t \tag{15}$$

with N_{step} the total number of calculated steps. It is thus readily seen that if $\dot{E}_{33_{imp}}$ is modified, the product $N_{step}\Delta t$ has to be modified as well to keep the first term of Eq. 15 constant. In many of the papers quoted above which deal with the influence of strain rate sensitivity, the macroscopic strain rate is rarely varied and only the influence of the exponent n is studied: it is for example mentioned by Canova and co-workers [1] that "all the results are normalized by the Von Mises (VM) equivalent strain-rate and are thus independent of the applied strain rate". In the present case, the grain VM equivalent strain rate indeed varies from grain to grain, for the selected boundary conditions (it would not be the case of course for the

FC assumption). The same expression is also valid at the macroscopic level, but if the material is macroscopically isotropic, it simply becomes equal to

$$\dot{E}_{VM} = \dot{E}_{33imp} \tag{16}$$

In the simulations performed below, we will thus have $\dot{\varepsilon}_{VM} \neq \dot{E}_{VM}$ in most of the grains. Also, as in many publications listed above, using either an homogenization model or a FE code, a reference case will be defined as the one performed by defining the reference shear rate equal to the macroscopic one, that is $\dot{\gamma}_0 = \dot{E}_{33imp}$, which means $\dot{E}_{33imp}/\dot{\gamma}_0 = \dot{E}_{VM}/\dot{\gamma}_0 = 1$. As a consequence, if the macroscopic strain rate $\dot{E}_{VM}$ is multiplied or divided by a factor of say 10, without modifying the value of the reference shear rate $\dot{\gamma}_0$, N_{step} will have to be divided or multiplied by 10, if $E_{33final}$ and Δt are kept constant. The exponent n will be varied in a wide range associated classically with room temperature deformation, i.e. between 10 and 200. This model will be used below to reproduce the mechanical behavior of several FCC materials (stainless steel and aluminum alloy) extracted from the literature. As in the selected examples, the texture is not documented or assumed to be isotropic, it is considered in the following only isotropic aggregates, represented by a set of 2016 orientations, uniformly distributed within the Euler space. For all treated examples, the 12 $111\langle 110\rangle$ systems will be considered. It is worth to point out that the aim of the present work is not to demonstrate the relevance of the RC Taylor model, but to be able to study the influence of the simple rate-sensitivity power law in a model allowing a strain rate gradient within the aggregate. Some tensile curves have been simulated with this approach to illustrate the influence of the various hardening parameters on the global response. These are shown in Figure 1, where it can be clearly seen that, for a given modelling approach, the initial value (resp. final value) of the macroscopic tensile stress is directly proportional to the value of $\tau_0 = \tau_{ini}$ (resp. τ_{sat}). This proportionality is even independent of the selected hardening law for the yield stress value.

3.2 The FE Abaqus code

As the objective is to deal with strain-rate sensitivity in the framework of FE codes, some simulations have also been performed with the FE code Abaqus, which is increasingly used for the simulation of the VP behavior of polycrystalline materials, with the very same description of the single crystal constitutive law. Again isotropic materials are considered. The simulation of a tensile test with such a code, however, is usually not performed with exactly

the same boundary conditions as the ones imposed in the RC Taylor model, since displacements, instead of strain rates, are generally applied in FE simulations. Furthermore, the description of the initial microstructure of the material is also somewhat different, since it accounts for both orientations and positions of the grains within polycrystalline aggregates, whereas only the orientation distribution is accounted for in the Taylor model.

In the present case, the considered isotropic material will be represented by a cubic polycrystalline aggregate of 200 grains, made of a Voronoï tessellation obtained from Neper program [41] and imported in Abaqus CAE using python scripts [42] (see Figure 2a). The grain boundaries are simply defined as the boundaries between zones of different orientations. The choice of a reduced number of orientations compared to the previous case appears here to be a good compromise to obtain both reasonable calculation times and a macroscopic uniaxial tensile stress, as with the RC Taylor model. The polycrystal is submitted to both symmetry boundary conditions and imposed displacement on the upper and lower faces, while on the lateral ones, uniform mixed-orthogonal (or block) conditions have been defined to account for periodicity [43, 44] (Figure 2b).

The crystal plasticity mechanical behavior, as defined in Eqs. 1 to 6, is introduced into Abaqus using a UMAT subroutine, which is extensively described in [33], and the Euler angle set (φ_1,Φ,φ_2) of each Voronoi cell is randomly determined in an ORIENT subroutine, describing thus an isotropic angle set.

4. Numerical results

4.1 Case study 1: the case of a rate-insensitive material

The first example treated with the simple RS constitutive law described above is the often encountered case of a material with a very low strain-rate sensitivity (represented by $1/n$). This in turns means a very high value of the n exponent. This exponent is usually established experimentally from flow stresses obtained at different strain rates but same microstructural state (e.g., dislocation density and thus same stress level), from the slope of the ln–ln stress–strain rate curve [45]:

$$n = \left.\frac{\partial \ln \dot{E}_M}{\partial \ln \Sigma}\right|_{\Sigma} \tag{17}$$

When doing so, values as high as 100–400 have been reported in the literature for various materials (copper, brass, many steels, ….) and this is why some regularized versions of the

present VP formulation have been proposed since calculations performed with very high values of n (above 200) are practically impossible to achieve, whatever the model used [29, 31]. Another way of solving this problem is to embed the norm of the applied strain rate into the reference shear rate $\dot{\gamma_0^s}$ [30], by imposing it to be equal to the applied macroscopic strain rate, i.e. $\dot{\gamma_0^s} = \dot{E}_{33imp}$ in the present case. It is then easy to show that in this case, the macroscopic response does not depend on the selected n value, and that the magnitude of the grain stress is affected only by the ratio of the grain strain rate magnitude and the macroscopic strain rate magnitude, which is not so large for FCC materials. This procedure is frequently used, especially when simulations are performed for one single macroscopic strain rate value.

Let us reproduce in this way, an experimental curve obtained at room temperature for a 304L stainless steel, whose texture is assumed to be isotropic [46]. In order to identify the hardening parameters for this case, the reference shear stress has been set equal to the actual strain rate, i.e., $0.001\ s^{-1}$, and the n exponent to 21, i.e. one of the value most often found in the literature "to reproduce negligible viscous behavior" [47] or for material which "possesses a certain rate-dependency at medium to high temperatures" [14, 34, 48-51]. The other material parameters have been manually identified on the experimental curve (see Figure 3); they are listed in Table I.

It is seen that, for the selected parameters, the agreement, although not 100% perfect, is quite satisfactory. An automatic identification procedure or the selection of a more physically-based hardening law would probably allow for a better fit over the whole strain range, but this is out of the scope of the present paper. Much more important, for it is the focus of the present study, it is seen that when $\dot{\gamma}_0 = \dot{E}_{VM}$, the influence of the exponent n is indeed very limited and negligible for $n \geq 21$, as reported in many studies using the same law.

But, once this reference case is satisfactorily treated, we may want to see what would happen if we change now the applied strain rate without changing the value of the reference shear stress $\dot{\gamma}_0$. This is illustrated in Figure 4, where simulations have been made using the parameters listed in Table 1, except for the applied normalized strain rate $\dot{E}_{VM}/\dot{\gamma}_0$ which has multiplied or divided by ten and the exponent n which has been varied from 21 to 111. It is seen that, when the normalized strain rate is set to $\dot{E}_{VM}/\dot{\gamma}_0 = 1/10$, there is an influence of the strain rate on the macroscopic response, and that the curves are almost superimposed only for $n \geq 91$. It is interesting to note that the best agreement with the experimental curve is now found for $n = 41$, which means that both reference strain rate $\dot{\gamma}_0$ and exponent n should

be considered simultaneously for the identification of the hardening parameters, as done in other works, see e.g. [9]: for the identification of the selected 304L tensile curve, taking $\dot{\gamma}_0 = 10 \times \dot{\mathrm{E}}_{VM}$ with $n = 41$ indeed provides a slightly better fit than $\dot{\gamma}_0 = \dot{\mathrm{E}}_{VM}$ with $n = 21$. It is also seen in Figure 4a that the overall stress level is increasing with n, when $\dot{\mathrm{E}}_{VM} < \dot{\gamma}_0$, as a consequence of the used power law.

If the normalized strain rate is set to $\dot{E}_{VM}/\dot{\gamma}_0 = 10$, there is again a clear influence of the strain rate on the macroscopic response, and the curves are again almost superimposed only for $n \geq 91$. The overall stress level is now decreasing when n increases, which better correspond to the expected influence of rate sensitivity and has already been observed in some other works: for example, these calculations are in full agreement with the ones performed by Khan et al. [9] with a similar power law.

Some curves obtained for two different values of n, namely 21 and 111 and various values of $\dot{E}_{33imp}/\dot{\gamma}_0$ between 1 and 10^{-4} (that is 4 orders of magnitude) are now presented in Figure 5. These curves have been obtained with the RC Taylor model as well as with Abaqus, with the same material parameters. For the FE simulation, as the elastic part of the curve is also simulated, the following elastic constants have been considered for 304L steel: C_{11}=197500 MPa, C_{22}=125000 MPa and C_{44}=122000 MPa. As the boundary conditions imposed to simulate a simple tensile test are not exactly expressed in the same way for the two approaches, before performing comparisons of the two sets of calculations, it has been checked that the macroscopic tensile test was indeed uniaxial in both cases (this would not have been necessarily the case for an anisotropic material). For comparison purposes, the elastic part of the curves has been taken out from the Abaqus simulations. It is interesting to note that the Abaqus curves are systematically below the RC Taylor curves, even though the Taylor model is not used in the pure FC mode (which would actually correspond to an upper bound). This means that the interactions between grains are softer in Abaqus than with the selected RC Taylor model. However, it is clear that the influence of the strain rate for given values of $\dot{\gamma}_0$ and n are similar for both approaches. It is also worth noting that $n \geq 111$, the convergence is very difficult to achieve with Abaqus, depending on the material description and imposed strain rate.

The influence of the normalized strain rate $\dot{E}_{VM}/\dot{\gamma}_0$ and strain rate sensitivity exponent n on the overall yield stress is now presented in Figure 6 for all performed situations. This yield stress is extracted at the first calculation step for the RC Taylor simulations and

evaluated at 0.02% plastic strain for the Abaqus simulations. Clearly this stress value does not vary much with the exponent for $\dot{E}_{VM}/\dot{\gamma}_0 = 1$ in both cases, but when this value is changed, the stress can strongly vary: for example, for n=21, the stress varies from about 180 to 310 MPa when $\dot{E}_{VM}/\dot{\gamma}_0$ varies from 0.0001 to 10 with the RC Taylor model; similarly, with Abaqus, the stress varies from 170 to about 263 MPa when $\dot{E}_{VM}/\dot{\gamma}_0$ varies from 0.0001 to 1. The response of the material is thus clearly rate-sensitive for n=21. The absence of strict linearity observed in the Abaqus simulations can be attributed to numerical reasons and to the local fluctuations of strain rate and stress, more significant than with the RC Taylor model, associated with weaker interactions between grains.

Now, by calculating the normalized ratio of this tensile yield stress by the reference shear stress (taken here equal to 100 MPa), the RC Taylor and Abaqus responses can be compared to the Upper and Lower Bounds rate-insensitive approaches. It is indeed well known that, for an isotropic FCC metal in the rate-insensitive limit, this normalized stress is equal to 3.06 for the upper bound (Taylor model), 2 for the lower bound (static model) and 2.2 for the Sachs – Kochendorfer model [52]. It is also clear from Figure 6, that this rate-insensitive value can be estimated for the viscoplastic RC Taylor and Abaqus models from the yield stress obtained for $\dot{E}_{VM} = \dot{\gamma}_0$ and the highest possible value for the exponent n. The so-obtained values are 2.78 for the RC Taylor model and about 2.62 for Abaqus. This confirms that the RC Taylor approximation is closer to the upper bound than to the lower one and that the interactions between grains are slightly softer with Abaqus. This also affects the hardening capacity as seen in Figure 5.

This first study has highlighted the fact that the only way to really neglect rate sensitivity with the power law is to set $\dot{\gamma}_0 = \dot{E}_{VM}$ and to keep the macroscopic strain rate constant; this is indeed well known from experienced users of VP mean field or full field methods, but much less from new FE codes users, if we look at the recent bibliography on the subject.

4.2 Case study 2: the case of a rate-sensitive material

Furthermore, if some alternatives exist to treat efficiently the case of the rate-insensitive materials, the simple power law (Eq. 1) is still largely used to treat the case of rate-sensitive materials within the static regime (typically for strain rates staying below 1.0 s^{-1}). Of course, as already said, it cannot alone account for the complex rate-sensitivity influence of a real material and the rate sensitivity of the hardening rate should also be considered [9, 32], especially if the treated problems involve strong flow localization [53, 54]. But, if it is not the

case, i.e. for moderate strains and strain rates, Christodoulou and Jonas [54] have shown that the use of the so-called continuous strain-rate sensitivity as defined by Eq. 17, i.e. determined at constant structural state, instead of a more instantaneous one, determined during strain rate change tests, compensates to some extent for the neglect of the rate sensitivity of hardening. Thus, even with a rather simple hardening law, by paying attention to the identification procedure, it can still reproduce quite precisely the observed behavior of materials tested at different strain rates and be useful for simulations for which strong localization is not expected. Let us take the example of pure aluminum (99.99%), which is more rate sensitive than the previously studied steel. Some experimental data have been extracted from [53, 54] and the rate sensitivity of the material has been estimated using Eq. 17 (Figure 7). The resulting estimated n value is found to be equal to 15 for an explored strain-rate range of 0.05 to 0.0005 s^{-1}.

Then, as in the previous example, the identification of the hardening parameters have been made for a reference case, corresponding to $\dot{\gamma}_0 = \dot{E}_{VM}$, arbitrarily selected equal to $0.0005\ s^{-1}$. We have also fixed the value of q to 1.1, classically selected for aluminum. Therefore, 3 parameters remain to be determined, which are $h_0, \tau_{ini}, \tau_{sat}$. These 3 parameters have been manually adjusted to reproduce the curve corresponding to $\dot{E}_{VM} = 0.0005\ s^{-1}$ and validated then by simulating the other curves corresponding to $\dot{E}_{VM} = 0.005\ s^{-1}$ and $\dot{E}_{VM} = 0.05\ s^{-1}$. The result of this first identification is presented in Table II and Figure 8a, in which the elastic parts of the experimental curves have been suppressed. In the validation process, the parameters may be slightly re-adjusted. In that case, they have to be validated again on the reference case.

Once the parameters have been selected for the whole explored strain-rate range, it may be desirable to modify the reference case, and thus the value of the associated reference strain-rate $\dot{\gamma}_0$. In that case, it is not necessary to perform the whole identification and validation process; it can simply be noticed that for a given model, the results of a 2nd identification procedure should coincide with the result of the 1st one, since the curves to be identified are precisely the same. In other words, if the material parameters are changed, the predicted stress and strain-rate tensors at the level of the grains as well as at the level of the sample should coincide at each step of the calculation and especially at the very beginning and at the saturation level (although this level may be not reached experimentally). From Eq. 3 and the definition of τ_{ini} and τ_{sat}, this implies that

$$\frac{\dot{\gamma}_0}{{\tau_{ini}}^n} = constant \quad \text{and} \quad \frac{\dot{\gamma}_0}{{\tau_{sat}}^n} = constant \tag{18}$$

from which the new values of τ_{ini} and τ_{sat} associated with the new selected value of $\dot{\gamma}_0$ can be extracted. There remains then one single parameter to be identified, namely the hardening coefficient h_0. The results of this procedure applied to the new reference case $\dot{\gamma}_0 = \dot{E}_{VM} = 0.05\ s^{-1}$ are also presented in Table 2 and Figure 8b. It is seen that the identified curves are very close to the ones obtained previously for the other set of parameters. Of course, for such a simple model, simulations are quite rapid (typically less than one minute for the calculation of one single curve in the presented examples), and thus the total identification procedure, whether performed manually as in the present case, or through an optimized identification procedure is also quite fast.

Contrary, for FE simulations, the identification of one set of parameters on one reference curve and the validation on the other two would take much longer times (depending on the computer). We can however accelerate the procedure if we first base our identification procedure for FE simulations on a preliminary identification step performed with a simpler model like the Taylor one as explained below.

In order to perform the identification of the 3 presented Al curves with Abaqus, it is first set again $n = 15$ and $q = 1.1$. The following elastic constants are also considered for aluminum: C_{11}=108240 MPa, C_{12}=62 160 MPa and C_{44}=28410 MPa. Then one reference case is selected, for example the same as previously, $\dot{\gamma}_0 = \dot{E}_{VM} = 0.0005\ s^{-1}$ and a first calculation is performed with Abaqus (s*im1*) **with the 3 hardening parameters issued from the RC Taylor identification**, called in the present case h_{01}, τ_{ini1}, τ_{sat1}. As the two approaches do not lead to the same response (see Figure 5), it is expected that the predicted curve will not perfectly fit the experimental one. One first correction can be made on τ_{ini} by using the proportionality relationship between initial stress σ_0 and τ_{ini}, illustrated in Figure 1, i.e.:

$$\frac{\sigma_{0sim1}}{\tau_{ini1}} = \frac{\sigma_{0exp}}{\tau_{ini}} \cong \frac{\sigma_{0Tay}}{\tau_{ini}} \tag{19}$$

In this expression, σ_{0Tay} represents the value of the yield stress estimated by the RC Taylor model. This equation allows us to immediately correct the value of τ_{ini} without any identification procedure. Once the beginning of the curve has been correctly adjusted, we can repeat the procedure for the saturation stress, by considering that, if this level is not reached on the experimental curves, it can be again correctly identified by the RC Taylor model, which means $(\sigma_{sat})_{Tay} \cong (\sigma_{sat})_{exp}$. The result of a 2nd Abaqus simulation (*sim2*) performed

with h_{01}, τ_{ini}, τ_{sat1} allows us to write

$$\frac{(\sigma_{sat})_{Tay}}{\tau_{sat}} = \frac{(\sigma_{sat})_{sim2}}{\tau_{sat1}} \tag{20}$$

and to obtain the correct value of τ_{sat} again without any identification procedure. It is worth noting, that this step implies to be able to perform one simulation with RC Taylor and one simulation with Abaqus up to the saturation level. This may involves convergence problems with Abaqus (especially if the saturation level is reached at very high strains). In this case, a classical identification procedure will have to be applied. In any case, there remains then one single parameter to be identified, which is again the hardening coefficient h_0. The procedure is summarized in Table III and illustrated in Figure 9. It is seen that the agreement between experimental and predicted curves is again quite satisfactory. Again, like for the RC Taylor model, some other materials parameters can be recalculated if we change the value of $\dot{\gamma}_0$ without being obliged to perform the simultaneous identification of all parameters.

4.3 Case study 3: the transition between static and dynamic regimes

The previous cases have illustrated clearly the fact that the macroscopic response of a polycrystalline aggregate strongly depends on both normalized strain rate (ratio of imposed over reference strain rates) and strain-rate sensitivity exponent; especially, the only configuration where a strain rate independent limit can be reached is for $\dot{E}_{VM} = \dot{\gamma}_0$, with n greater than 20). This is true when using simple mean field models such as the RC Taylor one (used here) as well as more complex full field tools such as FE codes. However, when FE simulations are performed, the strain rate, and thus the strain-rate sensitivity, can significantly vary from one point to another, as recently underlined by Shahba and Gosh [10] who studied the behavior of strongly anisotropic Ti alloys; in that case, the choice of the viscoplastic parameters $\dot{\gamma}_0$ and n is not so trivial if we want, e.g., to neglect the influence of strain rate in the whole sample. If one single macroscopic strain rate is investigated (and if the fluctuations within the simulated structure are expected to be moderate enough), then taking $\dot{E}_{VM} = \dot{\gamma}_0$ allows to neglect the strain rate sensitivity as much as possible and to select a n exponent as small as possible to reduce the computation time, without going to extensive multiple slip due to overestimated viscosity. Typically, a value around 20 satisfies these constraints and the hardening parameters can then be simply identified on one experimental curve (as done in the present case for the 304L material). But if several values of macroscopic or microscopic strain rate need to be considered, then the selection of the two parameters can be made according to

several procedures:

(i) As suggested by Khan et al. [9], it is possible to arbitrarily select for $\dot{\gamma}_0$ one of the investigated values of strain rate and to identify the hardening parameters on the corresponding curve and then, to identify the n exponent on the curves obtained for the other strain rates. According to these authors however, this option is not completely satisfactory if the associated hardening law is too simplified, as the one used in the present work, since they argue that it is not possible in this case to reproduce all experimental curves obtained e.g. on aluminum single crystals over a wide range of strain rate with one single n parameter. They then propose to select a more complex hardening law, which comprises an additional strain rate sensitivity parameter. It is worth mentioning though that the behavior of the tested Al single crystals observed at varying strain rates is somewhat in contradiction with the conclusions drawn recently by Shahba and Gosh [10] who claimed that in general (and not only for the Ti alloys), the classical phenomenological power law is valid up to larger strain rates (up to 10^4 s^{-1}) than the ones investigated by Khan et al. [8], which do not exceed 10^3 s^{-1}.

(ii) Alternatively, it can be recognized, as suggested by Canova et al. already in 1988 [1] and more recently by Uenishi and Teodosiu [55] or by Shahba and Gosh [10], that one single n parameter cannot reproduce all observed behaviors and that there are indeed three different regimes:

1. the quasi-static regime associated with strain rates below 1 s^{-1},
2. the dynamic regime associated with strain-rates typically above 100 or even 1000 s^{-1} – depending on the authors – these two regimes being associated either with significantly different values of n or with different VP flow rules and even different hardening mechanisms [10, 55],
3. the transition regime between the two, within which the n value may vary more or less smoothly.

To describe this evolution from quasi-static to dynamic regime, Canova et al. [1] proposed a bilinear expression for the evolution of the true stress as a function of the strain rate whereas Uenishi and Teodosiu [55] proposed a parabolic expression, taking into account the effect of temperature within the dynamic regime. As for Shahba and Gosh [10], they propose a so-called unified flow-rule, applicable to a very wide range of applied strain-rates and temperatures, "uniquely capable of seamlessly accounting for the effects of location-dependent thermally-activated (at low strain rates) and drag-dominated (at high strain rates)

mechanisms of dislocation glide without any user intervention". Their law is thus especially well adapted to FE simulations performed for very high strain rates, for which strain rates at different locations in a heterogeneous polycrystalline microstructure are expected to vary significantly even for a uniformly applied macroscopic strain-rate.

If the existence of two different regimes (and possibly of a smooth transition between the two) is thus well recognized, it is then easy to conclude that the use of the classical VP flow rule with one single set of parameters (describing both flow and hardening rules) should be allowed within one of these two regimes only. As long as the influence of temperature is not explicitly included, as e.g. in the phenomenological hardening law selected in the present work, it is also easy to recognize that the present formulation is thus more adapted to the quasi-static regime than to the dynamic one (for which additional microscopic deformation mechanisms are expected to occur). In this case, the value of $\dot{\gamma}_0$ should also be selected within the quasi-static regime, which means typically below 1 s^{-1}. If the parameters are identified as previously explained, it is then possible to reproduce the behavior of a material within the whole quasi-static regime with one single set of parameters, as already illustrated for polycrystalline aluminum in section 4.2 but also for Al single crystals, as illustrated in Figure 10: the experimental curves obtained on Al single crystals deformed in compression by Khan et al. [9] have been reproduced with the RC Taylor model (see parameters in Table IV). It is seen that the 3 curves corresponding to the quasi-static regime are well reproduced (even better than in the original paper with a different, although also phenomenological hardening law) whereas the one associated with the dynamic regime (strain rate equal to 1000 s^{-1}) is not with the quasi-static parameters. If now the n exponent is allowed to be modified for the dynamic regime, then the curve can also be reproduced with the simple RC Taylor model and saturating hardening law. It is worth mentioning though, that the strain-rate sensitivity ($1/n$) is observed here to decrease at high strain rate, in contradiction with most of the other observations performed in metals [1, 10, 20, 33, 55, 56]. The reason for this quite unusual dynamic behavior of the tested Al single crystals is not explained in ref. [8].

6. Conclusions

The aim of the present study was to rationalize the use of the simple VP power law, still widely used for its simplicity with mean field and full field approaches to model the behavior of polycrystalline samples in a wide range of strain-rates or temperatures. For this purpose,

one mean field (RC Taylor model) and one full field (Abaqus FE code) approaches have been selected, with the very same description of the single crystal behavior (fcc in the present case). These two approaches have been selected since they can predict heterogeneities of strain, stress and strain rate within a polycrystalline sample, as experimentally observed. As a consequence, the conclusions drawn below are thought to be also applicable to other modelling choices. Through the simulation of simple tensile tests and the comparison of some simulated and experimental curves, we have shown that:

(i) with such a rate-sensitive single crystal constitutive law, it is possible to simulate the behavior of rate-sensitive or rate-insensitive materials, in the framework of both mean field or full field approaches, provided that it is remembered that the macroscopic response of a polycrystalline aggregate will depend on both values selected for the reference strain rate $\dot{\gamma}_0$ with respect to the imposed one and the strain-rate sensitivity exponent n;

(ii) for rate-insensitive materials, the strain-rate exponent value which allows to approximate the rate-insensitive limit with sufficient precision depends on the macroscopic strain rate, as long as the $\dot{\gamma}_0$ parameter has been selected. If $n = 21$ is high enough for a strain rate equal to $\dot{\gamma}_0$, much higher values must be selected, as soon as the strain rate is modified; as a consequence, even for $n = 21$ and $\dot{E}_{VM} = \dot{\gamma}_0$, some strain rate sensitivity can be observed within individual grains, as long as the deformation is not prescribed to be uniform within the whole polycrystalline sample and that strain-rate variations are thus observed; today, this is well-known only by a limited part of the FE code users;

(iii) the VP formulation with one single exponent and associated with a simple hardening law neglecting the temperature effects, is quite adequate to describe the quasi-static regime, i.e. typically for strain rates below 1/s (or below $\dot{\gamma}_0$), for rate-sensitive materials; once all parameters have been identified for one reference case, it is then easy to modify them to treat another reference case. It has been shown that the identification procedure can be considerably simplified in this case, since 2 of the 3 hardening parameters can simply be corrected without any identification procedure;

(iv) the identification of all parameters of the constitutive law with an FE code can be greatly accelerated by relying on the identification previously carried out with a simpler model, such as the RC Taylor model.

(v) The simple VP formulation studied here can also be used to describe the behavior of rate-sensitive material in an extended range of strain-rate (i.e. including both static and dynamic regimes), provided that the exponent n is identified separately in both regimes.

Finally, it is worth recalling that this widely used VP formulation is phenomenological. It is thus not adequate to describe completely all the microscopic mechanisms. If this is desired, this simple formulation should be enriched to account for a more precise description and more detailed understanding of strain rate and temperature effects.

Acknowledgments

The authors acknowledge the help of H.T. Nguyen, B. Sadriji and A.M. Karadaniz (former Univ. Sorbonne Paris Nord Students) for their contribution in the realization of a UMAT subroutine. This work has benefited from financial support from the LABEX SEAM through the National Research Agency under the "Investissements d'Avenir program" with the reference numbers ANR-11-LABX-086 and ANR-11-IDEX- 0005-02.

Two of the authors (YC and BB) have learned a lot about the use of Abaqus from P. Gilormini, with whom they have both already had the opportunity to publish research based on the advanced use of the code. They were able to appreciate and share his constant questioning on how the code is implemented, its limits and the way to overcome them, his expertise on writing and decrypting UMATs, and his deep competence also on crystal viscoplasticity. The present paper is partly a legacy of these previous collaborations with P. Gilormini.

References

1. Canova, G.R., C. Fressengeas, A. Molinari, and U.F. Kocks, *Effect of rate sensitivity on slip system activity and lattice rotation.* Acta Metallurgica, 1988. **36**(8): p. 1961-1970.
2. Toth, L.S., P. Gilormini, and J.J. Jonas, *Effect of rate sensitivity on the stability of torsion textures.* Acta Metallurgica, 1988. **36**(12): p. 3077-3091.
3. Taylor, G.I., *The Mechanism of Plastic Deformation of Crystals. Part I. Theoretical.* Proceedings of the Royal Society of London. Series A, 1934. **145**(855): p. 362–87.
4. Lebensohn, R.A., C.N. Tome, and P.P. Castaneda, *Self-consistent modelling of the mechanical behaviour of viscoplastic polycrystals incorporating intragranular field*

fluctuations. Philosophical Magazine, 2007. **87**(28): p. 4287-4322.
5. Hutchinson, J.W., *Bounds and Self-Consistent Estimates for Creep of Polycrystalline Materials.* Proceeding Royal Society London, 1976. **A 348**: p. 101-127.
6. Beyerlein, I.J. and C.N. Tomé, *Modeling transients in the mechanical response of copper due to strain path changes.* International Journal of Plasticity, 2007. **23**(4): p. 640-664.
7. Phan, V.-T., T.-D. Nguyen, Q.-H. Bui, and G. Dirras, *Modelling of microstructural effects on the mechanical behavior of ultrafine-grained Nickel using crystal plasticity finite element model.* International Journal of Engineering Science, 2015. **94**: p. 212-225.
8. Klusemann, B., B. Svendsen, and H. Vehoff, *Investigation of the deformation behavior of Fe–3%Si sheet metal with large grains via crystal plasticity and finite-element modeling.* Computational Materials Science, 2012. **52**(1): p. 25-32.
9. Khan, A.S., J. Liu, J.W. Yoon, and R. Nambori, *Strain rate effect of high purity aluminum single crystals: Experiments and simulations.* International Journal of Plasticity, 2015. **67**: p. 39-52.
10. Shahba, A. and S. Ghosh, *Crystal plasticity FE modeling of Ti alloys for a range of strain-rates. Part I: A unified constitutive model and flow rule.* International Journal of Plasticity, 2016. **87**: p. 48-68.
11. Monnet, G., L. Vincent, and B. Devincre, *Dislocation-dynamics based crystal plasticity law for the low- and high-temperature deformation regimes of bcc crystal.* Acta Materialia, 2013. **61**(16): p. 6178-6190.
12. Shanthraj, P. and M.A. Zikry, *Dislocation density evolution and interactions in crystalline materials.* Acta Materialia, 2011. **59**(20): p. 7695-7702.
13. Asaro, R.J., *Crystal Plasticity.* J Appl Mech., 1983. **50**: p. 921-14.
14. Hill, R. and J.R. Rice, *Constitutive analysis of elastic-plastic crystals at arbitrary strain.* Journal of the Mechanics and Physics of Solids, 1972. **20**: p. 401-413.
15. Miehe, C. and J. Schröder, *A comparative study of stress update algorithms for rate-independent and rate-dependent crystal plasticity.* International Journal for Numerical Methods in Engineering, 2001. **50**: p. 273-298.
16. Hutchinson, J.W. and K.W. Neale, *Influence of strain-rate sensitivity on necking under uniaxial tension.* Acta Metallurgica, 1977. **25**(8): p. 839-846.
17. Vadillo, G., J.A. Rodríguez-Martínez, and J. Fernández-Sáez, *On the interplay between strain rate and strain rate sensitivity on flow localization in the dynamic expansion of ductile rings.* International Journal of Solids and Structures, 2012. **49**(3–4): p. 481-491.
18. Zhou, F., J.F. Molinari, and K.T. Ramesh, *Effects of Material Properties and Strain Rate on the Fragmentation of Brittle Materials.* International Journal of Fracture, 2006. **139**: p. 169-196.
19. Asaro, R.J. and A. Needleman, *Overview no. 42 Texture development and strain hardening in rate dependent polycrystals.* Acta Metallurgica, 1985. **33**(6): p. 923-953.
20. Klopp, R.W., R.J. Clifton, and T.G. Shawki, *Pressure-shear impact and the dynamic viscoplastic response of metals.* Mechanics of Materials, 1985. **4**(3): p. 375-385.
21. Leng, Z., H. Pan, Z. Niu, C. Guo, Q. Zhang, Y. Chang, M. Zhang, and F. Jiang, *Mechanical behavior, deformation and damage mechanisms of Mg–RY–Zn alloy under high strain rate.* Materials Science and Engineering: A, 2016. **651**: p. 336-340.
22. Bintu, A., G. Vincze, R.C. Picu, and A.B. Lopes, *Effect of symmetric and asymmetric rolling on the mechanical properties of AA5182.* Materials & Design, 2016. **100**: p. 151-156.
23. Luo, J., M. Li, W. Yu, and H. Li, *The variation of strain rate sensitivity exponent and*

strain hardening exponent in isothermal compression of Ti–6Al–4V alloy. Materials & Design, 2010. **31**(2): p. 741-748.
24. Luo, J., J. Gao, L. Li, and M.Q. Li, *The flow behavior and the deformation mechanisms of Ti–6Al–2Zr–2Sn–2Mo–1.5Cr–2Nb alloy during isothermal compression.* Journal of Alloys and Compounds, 2016. **667**: p. 44-52.
25. Mao, Z.N., X.H. An, X.Z. Liao, and J.T. Wang, *Opposite grain size dependence of strain rate sensitivity of copper at low vs high strain rates.* Materials Science and Engineering: A, 2018. **738**: p. 430-438.
26. Peroni, L. and M. Scapin, *Experimental analysis and modelling of the strain-rate sensitivity of sheet niobium.* EPJ Web Conf., 2018. **183**: p. 01014.
27. Rusinek, A., J.A. Rodríguez-Martínez, and A. Arias, *A thermo-viscoplastic constitutive model for FCC metals with application to OFHC copper.* International Journal of Mechanical Sciences, 2010. **52**(2): p. 120-135.
28. Fréchard, S., A. Redjaïmia, E. Lach, and A. Lichtenberger, *Dynamical behaviour and microstructural evolution of a nitrogen-alloyed austenitic stainless steel.* Materials Science and Engineering: A, 2008. **480**(1): p. 89-95.
29. Knezevic, M., M. Zecevic, I.J. Beyerlein, and R.A. Lebensohn, *A numerical procedure enabling accurate descriptions of strain rate-sensitive flow of polycrystals within crystal visco-plasticity theory.* Computer Methods in Applied Mechanics and Engineering, 2016. **308**: p. 468-482.
30. Kok, S., A.J. Beaudoin, and D.A. Tortorelli, *A polycrystal plasticity model based on the mechanical threshold.* International Journal of Plasticity, 2002. **18**(5): p. 715-741.
31. Forest, S. and M.B. Rubin, *A rate-independent crystal plasticity model with a smooth elastic–plastic transition and no slip indeterminacy.* European Journal of Mechanics - A/Solids, 2016. **55**: p. 278-288.
32. Zecevic, M. and M. Knezevic, *A new visco-plastic self-consistent formulation implicit in dislocation-based hardening within implicit finite elements: Application to high strain rate and impact deformation of tantalum.* Computer Methods in Applied Mechanics and Engineering, 2018. **341**: p. 888-916.
33. Huang, Y., *A User-Material Subroutine Incorporating Single Crystal Plasticity in the ABAQUS Finite Element Program.* 1991: Unknown.
34. Hu, L., S. Jiang, Y. Zhang, and D. Sun, *Crystal plasticity finite element simulation of NiTi shape memory alloy based on representative volume element.* Met. Mater. Int., 2017. **23**: p. 1075.
35. Peirce, D., R.J. Asaro, and A. Needleman, *An analysis of nonuniform and localized deformation in ductile single crystals.* Acta Metallurgica, 1982. **30**(6): p. 1087-1119.
36. Asaro, R.J., *Micromechanics of Crystals and Polycrystals*, in *Advances in Applied Mechanics*, W.H. John and Y.W. Theodore, Editors. 1983, Elsevier. p. 1-115.
37. Arminjon, M. and B. Bacroix, *On plastic potentials for anisotropic metals and their derivation from the texture function.* Acta Mechanica, 1991. **88**(3-4): p. 219-243.
38. Sachs, G., *Zur Ableitung einer Filebedingung.* Zeitschrift des Vereines Deutscher Ingenieure, 1928. **72**: p. 734-736.
39. Kochendorfer, A., *Plastiche Eigenschaften von Kristallen und Metallischen Werkstoffen.* 1941, Berlin: Springer.
40. Bacroix, B., S. Queyreau, D. Chaubet, E. Siv, and T. Chauveau, *The influence of the cube component on the mechanical behaviour of copper polycrystalline samples in tension.* Acta Materialia, 2018. **160**: p. 121-136.
41. Quey, R., P.R. Dawson, and F. Barbe, *Large-scale 3D random polycrystals for the finite element method: Generation, meshing and remeshing.* Computer Methods in Applied Mechanics and Engineering, 2011. **200**(17): p. 1729-1745.

42. Simulia, *Abaqus Scripting User's Manual*, 2011a.
43. Salahouelhadj, A. and H. Haddadi, *Estimation of the size of the RVE for isotropic copper polycrystals by using elastic-plastic finite element homogenisation.* Computational Materials Science, 2010. **48**(3): p. 447-455.
44. Charles, Y., R. Estevez, E. Maire, and Y. Brechet, *Modelling the competition between interface debonding and particle fracture using a plastic strain dependent cohesive zone.* Engineering Fracture Mechanics, 2010. **77**(4): p. 705-718.
45. Hosford, W.F., *Mechanical Behaviour of Materials*. 2010, New York, NY, USA: Cambridge University Press.
46. Chavez, S.A., G.E. Korth, D.M. Harper, and T.J. Walker, *High-temperature tensile and creep data for Inconel 600, 304 stainless steel and SA106B carbon steel.* Nuclear Engineering and Design, 1994. **148**(2): p. 351-363.
47. El Shawish, S. and L. Cizelj, *Combining Single-and Poly-Crystalline Measurements for Identification of Crystal Plasticity Parameters: Application to Austenitic Stainless Steel.* Crystals, 2017. **7**: p. 181.
48. Zhang, Y., S. Jiang, L. Hu, Y. Zhao, and D. Sun, *Investigation of primary static recrystallization in a NiTiFe shape memory alloy subjected to cold canning compression using the coupling crystal plasticity finite element method with cellular automaton.* Modelling and Simulation in Materials Science and Engineering, 2017. **25**: p. 075008.
49. Teferra, K. and L. Graham-Brady, *A random field-based method to estimate convergence of apparent properties in computational homogenization.* Computer Methods in Applied Mechanics and Engineering, 2018. **330**: p. 253-270.
50. Hu, L., S. Jiang, T. Zhou, J. Tu, L. Shi, Q. Chen, and M. Yang, *Multiscale Modeling of Polycrystalline NiTi Shape Memory Alloy under Various Plastic Deformation Conditions by Coupling Microstructure Evolution and Macroscopic Mechanical Response.* Materials & Design, 2017. **10**: p. 1172.
51. Zhao, L., P. Chakraborty, M.R. Tonks, and I. Szlufarska, *On the plastic driving force of grain boundary migration: A fully coupled phase field and crystal plasticity model.* Computational Materials Science, 2017. **128**: p. 320-330.
52. Belkhabbaz, A., B. Bacroix, and R. Brenner, *Investigation of the elastoplastic behavior of FCC polycrytals using a FFT numerical scheme.* Roumanian Journal Techn. Sci. – Appl. Mechanics, 2015. **60**: p. 5–23.
53. Christodoulou, N. and J.J. Jonas, *Flow localization in OFHC Cu and 99.99% Al.* Acta Metallurgica, 1985. **33**(4): p. 719-719-730.
54. Christodoulou, N. and J.J. Jonas, *Work hardening and rate sensitivity material coefficients for OFHC Cu and 99.99% Al*, 1984. p. 1655-1655-68.
55. Uenishi, A. and C. Teodosiu, *Constitutive modelling of the high strain rate behaviour of interstitial-free steel.* International Journal of Plasticity, 2004. **20**: p. 915-936.
56. Campbell, J.D., *Dynamic Plasticity of Metals*, ed. U. CISM. 1970, Berlin: Springer.

Table I. Imposed and adjusted parameters for the identification of the 304L experimental curve with the RC Taylor model.

Imposed test conditions (reference case)	$\dot{E}_{VM} = \dot{E}_{33imp} = 0.001\ s^{-1}$ $E_{33max} = 0.35$
Imposed parameters	$\dot{\gamma_0^s} = \dot{\gamma_0} = 0.001\ s^{-1}$ $n = 21$
Material adjusted parameters	$\tau_0^s = 100\ MPa$ $h_0 = 260\ MPa, q = 1.1$ $\tau_{sat} = 300\ MPa, \tau_{ini} = 100\ MPa$

Table II. Imposed and adjusted parameters for the identification of the aluminum experimental curves with the RC Taylor model.

$\dot{E}_{VM}$ (s^{-1}) for the identified curve	Imposed parameters			Adjusted parameters		
	n	$\dot{\gamma_0}$ (s^{-1})	q	h_0 (MPa)	τ_{ini} (MPa)	τ_{sat} (MPa)
0.0005	15	0.0005	1.1	4	15	35
0.05	15	0.05	1.1	5.7	20	47

Table III. Imposed and adjusted parameters for the identification of the aluminum experimental curves with the Abaqus FE code.

Simulation	Fixed parameters n = 15, $\dot{E}_{VM} = \dot{\gamma_0} = 0.0005\ s^{-1}$, q = 1.1			
	Parameters to be identified	h_0 (MPa)	τ_{ini} (MPa)	τ_{sat} (MPa)
sim1 (up to σ_0)	h_{01}, τ_{ini1}, τ_{sat1} issued from the RC Taylor identification	4	15	35
sim2 (up to σ_{sat})	τ_{ini} corrected by Eq. 19 h_{01}, τ_{sat1} issued from the RC Taylor identification	4	14	35
sim3 (up to $\sigma_{expfinal}$)	τ_{sat} corrected by Eq. 20 Identification of h_0 with Abaqus	5	14	45

Table IV. Imposed and adjusted parameters for the identification of the Al single crystals compression curves of Khan et al. [9] with the RC Taylor model.

Imposed test conditions	$\dot{E}_{VM} = \dot{E}_{33imp} = 1$ to $0.001\ s^{-1}$ (quasi-static) $\dot{E}_{VM} = \dot{E}_{33imp} = 1000\ s^{-1}$ (dynamic)
Reference case for identification of the material parameters	$\dot{E}_{33imp} = 1$
Imposed parameters	$\dot{\gamma_0^s} = \dot{\gamma}_0 = 1\ s^{-1}$ $n = 21$(quasi-static), $n = 41$ (dynamic)
Adjusted parameters	$\tau_0^s = 5\ MPa$ $h_0 = 40\ MPa, q = 1.1$ $\tau_{sat} = 35\ MPa, \tau_{ini} = 5\ MPa$

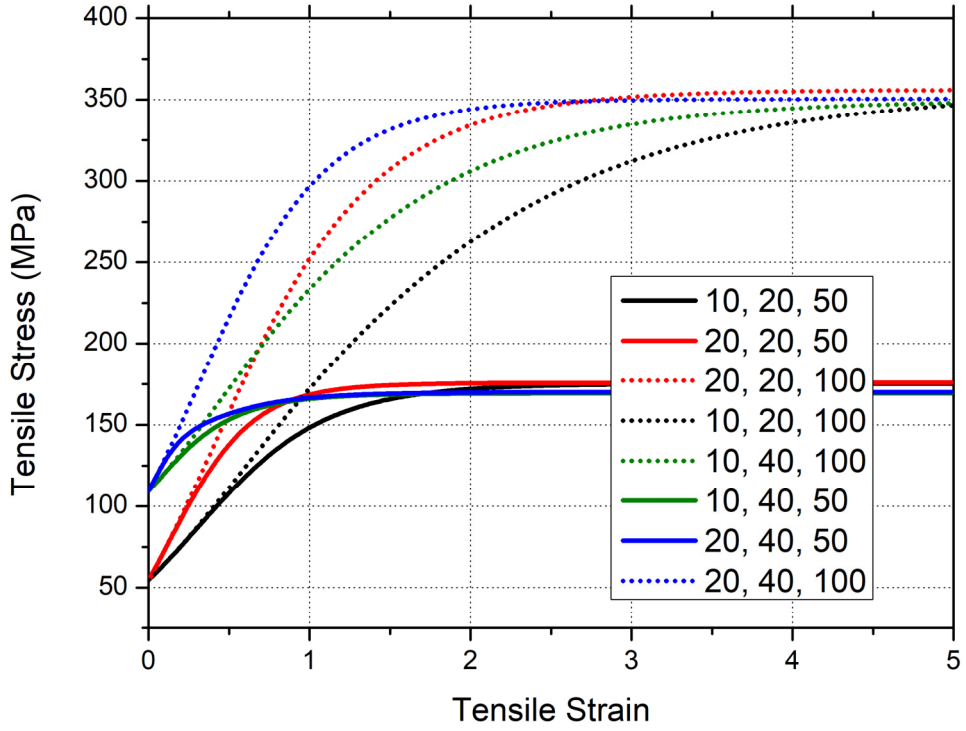

Figure 1. Simulated tensile curves using the RC Taylor model, with $\dot{\gamma_0^s} = \dot{\gamma}_0 = \dot{E}_{VM} = 0.0005\ s^{-1}$, $q = 1.1$ and $n = 21$. The 3 hardening parameters h_0, τ_{ini}, τ_{sat} are varied and their values (in MPa) given in the figure legend.

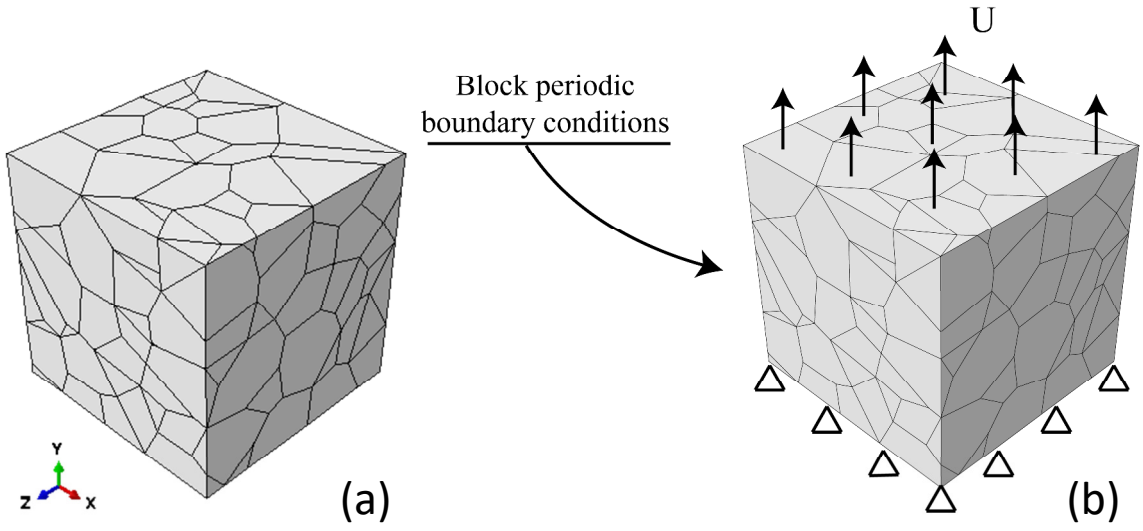

Figure 2. (a) Example of a Voronoi tessellation made of 200 grains and (b) applied boundary conditions.

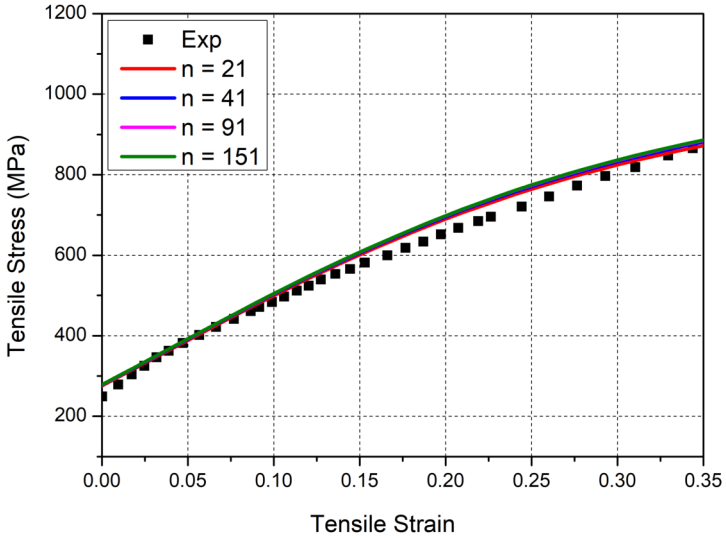

Figure 3. Tensile curves obtained with the RC Taylor model for the reference case ($\dot{E}_{33imp}/\dot{\gamma}_0 = \dot{E}_{VM}/\dot{\gamma}_0 = 1$) and various n values. Comparison with the experimental curve obtained by Chavez et al. [46] on a 304L stainless steel at room temperature.

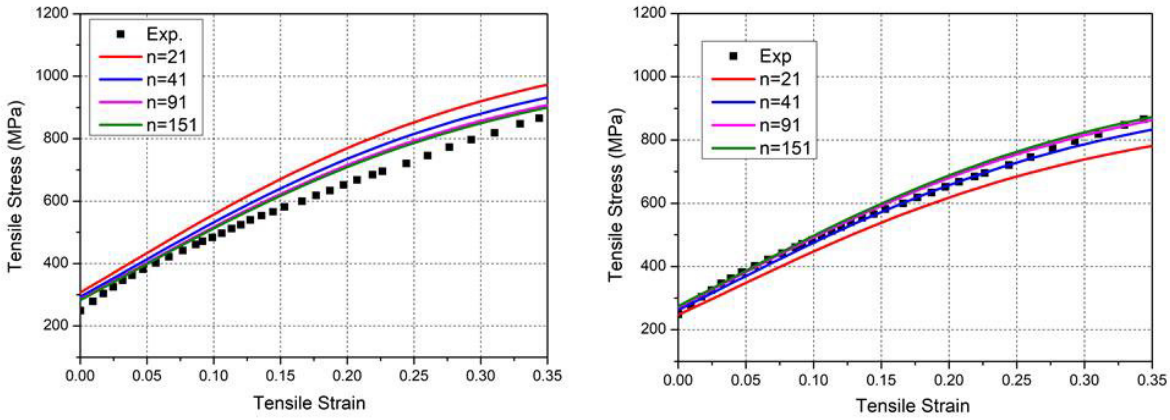

(a) $\dot{E}_{VM}/\dot{\gamma}_0 = 1/10$ (b) $\dot{E}_{VM}/\dot{\gamma}_0 = 10$

Figure 4. Tensile curves obtained with the RC Taylor model for 2 test parameter sets different from the reference case, and various n values. Comparison with the experimental curve obtained by Chavez et al. [46] on a 304L stainless steel at room temperature.

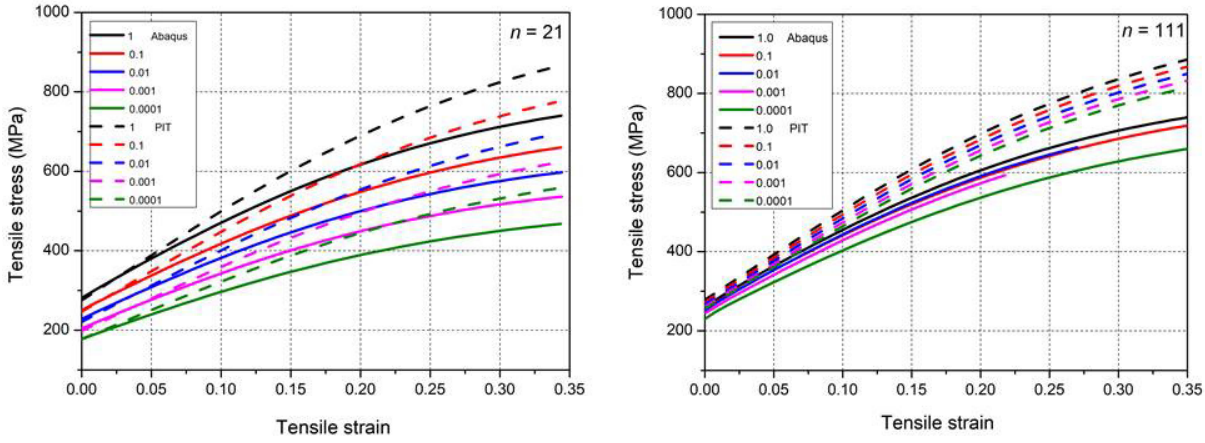

Figure 5. Tensile curves obtained with the RC Taylor model and the Abaqus code for 5 different applied normalized strain rate values (from 0.0001 up to 1 s^{-1}) and n=21 or 111.

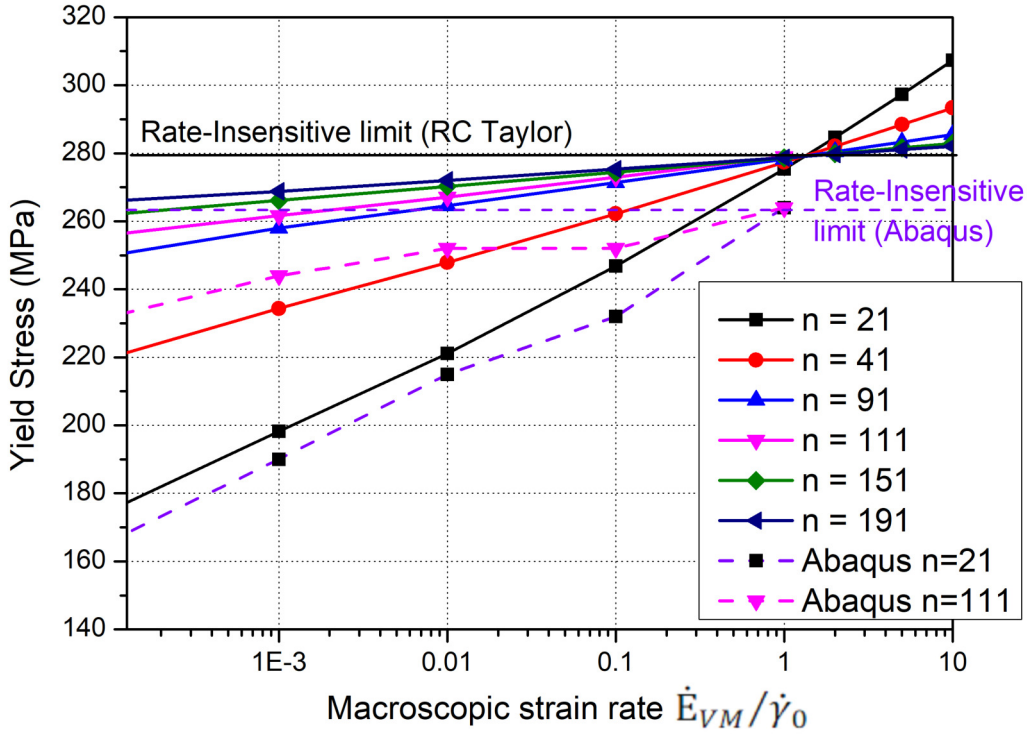

Figure 6. Evolution of the macroscopic yield stress as a function of strain rate and strain-rate sensitivity exponent for all performed simulations.

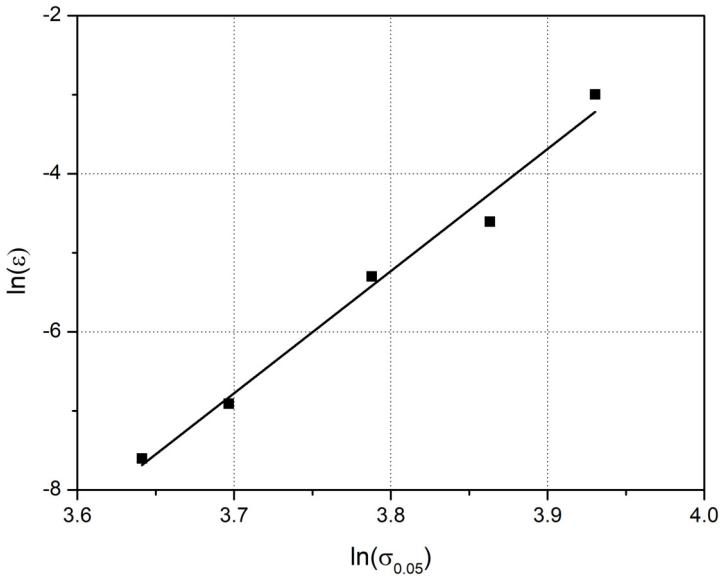

Figure 7. Relationship between strain rate and yield stress extracted from experimental tensile curves obtained on pure aluminum at room temperature [54].

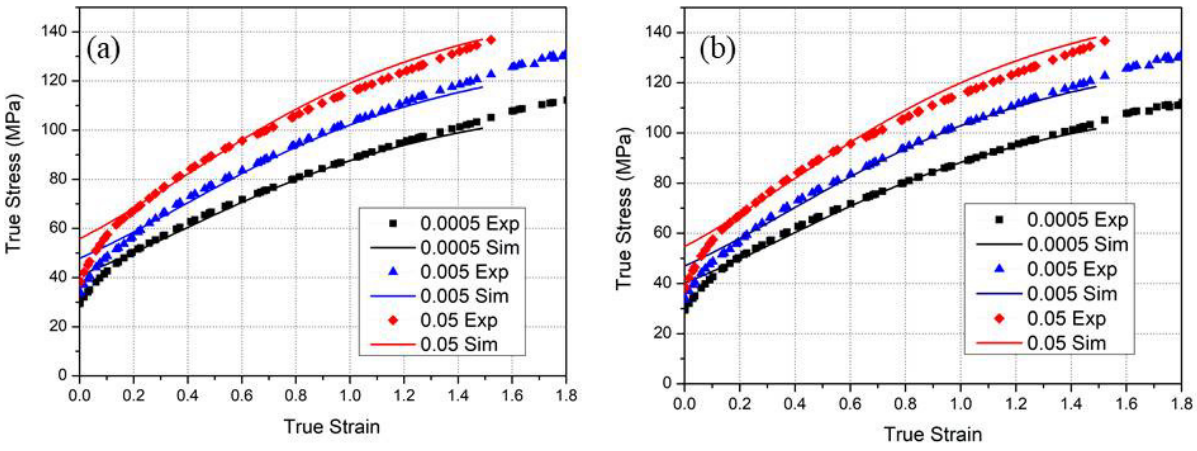

Figure 8. Stress – strain curves obtained for pure aluminum deformed in tension at various strain rates. The experimental curves are taken from [54] and the simulated ones are obtained with the RC Taylor model, using 2 sets of parameters (see Table II): (a) $\dot{\gamma}_0 = 0.0005\ s^{-1}$ and (b) $\dot{\gamma}_0 = 0.05\ s^{-1}$.

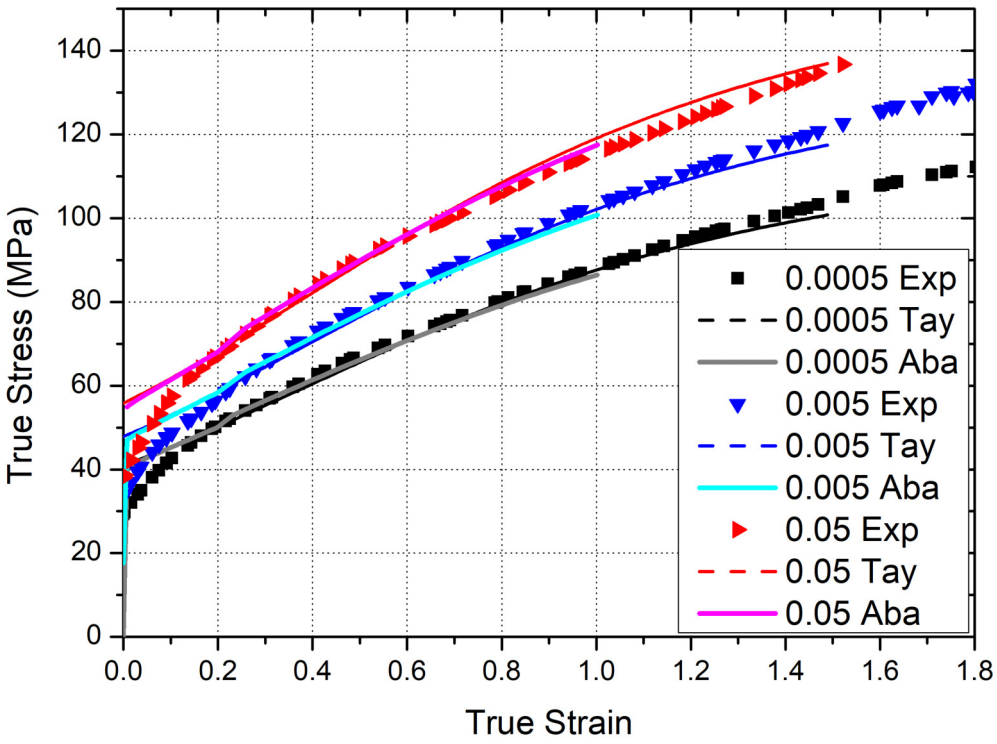

Figure 9. Stress – strain curves obtained for pure aluminum deformed in tension at various strain rates. The experimental curves are taken from [53] and the simulated ones are obtained with the RC Taylor model (parameters in Table II) and with the Abaqus FE code, with the hardening parameters listed in Table III, evaluated with the proposed identification method.

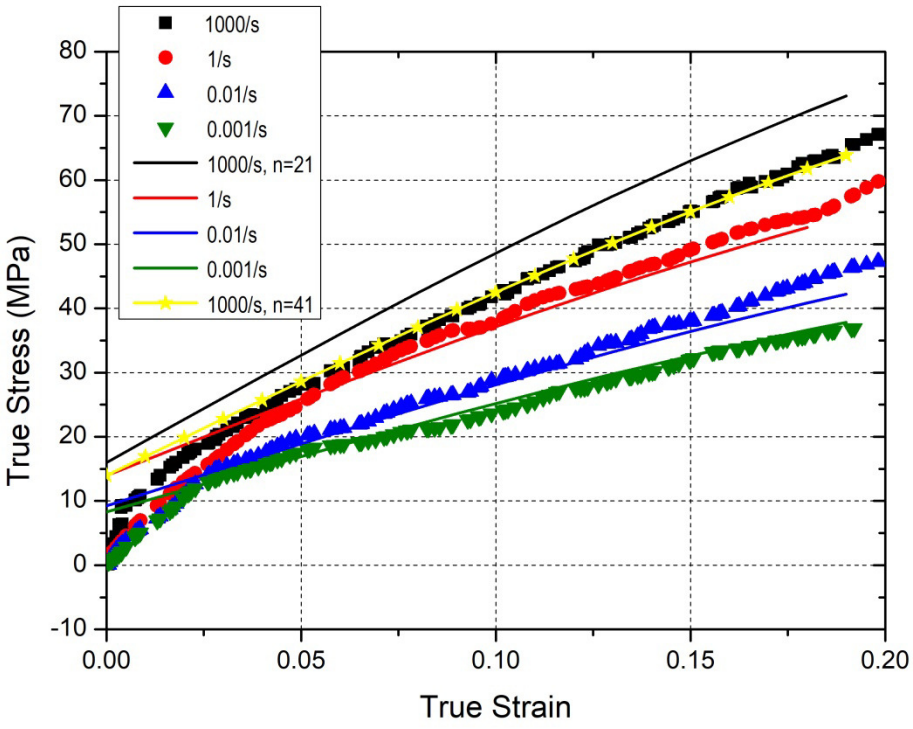

Figure 10. Experimental (dotted lines from [9]) and simulated (full lines, RC Taylor model) curves for Al single crystals deformed in compression.